INTERNATIONAL JOURNAL FOR NUMERICAL METHODS IN FLUIDS, VOL. 18, 437–447 (1994)

CALCULATION OF SEPARATED FLOW AROUND MULTI-ELEMENT AEROFOILS USING CONFORMAL MAPPING

JIANFA CAO*

Beijing University of Aeronautics and Astronautics, Beijing 100083, China

SUMMARY

A method is presented to calculate the low-speed incompressible separated flow around multi-element aerofoils. The geometries of multi-element aerofoils in the physical plane are completely arbitrary and are transformed into multiple circles in the computational plane by a conformal mapping technique. Jacob's model, which distributes sources on the separated surfaces of multi-element aerofoils to simulate the effects of separation, is adopted here. The position of the separated point and the pressure on the surfaces of multi-element aerofoils are calculated by iteratively coupling the potential flow and boundary layer. The effects of the boundary layer are simulated by modification of the boundary condition. All iterative procedures converge rapidly as a result of using the fast Fourier transform (FFT) technique.

KEY WORDS Multi-element aerofoils Separated flow Fast Fourier transform Conformal mapping

1. INTRODUCTION

The numerical simulation of separated flow about multi-element aerofoils is a very important problem for the development of a high-lift system for a specific flight vehicle and mission. So far it has been carried out mainly in two ways: first, by numerical calculation of the complete Navier–Stokes (N–S) equations or an appropriate approximation of them; second, by assuming a physical model for the separated flow and then solving for the mathematical solution. In order to get an accurate representation of all phenomena connected with the complicated flow field introduced by flap deployment, it is necessary to employ fine grids with strong stretching near boundaries; thus the simulation of viscous separated flow around multi-element aerofoils by numerical solution of the N–S equations usually requires much computation time.[1–5] For the second formulation Jacob[6] did the initial research using a source or source distribution in the aft region of the aerofoils to form the separated region. Later this idea was adopted by a number of researchers with various modifications (see e.g. References 7–9). At present this is the method most commonly used to calculate the separated flow about aerofoils because of its comparatively better computational efficiency.

This paper presents a new method to calculate the separated flow around multi-element aerofoils using conformal mapping and fast Fourier transform techniques. In this method the multi-element aerofoils in the physical plane are first transformed into multiple circles in the

* Present address: Department of Mechanical and Aeronautical Engineering, Clarkson University, Potsdam, NY 13699, U.S.A.

CCC 0271–2091/94/050437–11

Received 14 May 1993
Revised 26 September 1993

computational plane; the flow solution is then calculated in the computational plane and finally transformed back to the physical plane. The flow is assumed to be incompressible and steady. The effects of the confluent boundary layer are neglected in the calculation. Jacob's method is used to model the separated flow about the multi-element aerofoils. The strength of sources distributed on the separated surfaces of the multi-element aerofoils is determined by taking the pressure as constant in separated regions above these surfaces. Boundary layer displacement effects are simulated by modification of the boundary condition that specifies the non-zero normal velocity distribution.

The following sections give more details about this method.

2. CONFORMAL MAPPING OF MULTI-ELEMENT AEROFOILS

2.1. Conformal mapping of a single-element aerofoil

The purpose of conformal transformation is to map an aerofoil in the physical plane Z conformally on to a unit circle in the computational plane ξ.

Because the trailing edge point of the aerofoil is a singular point, a Karman–Treffez transformation is first introduced to map the aerofoil in the Z-plane on to a smooth quasi-circle in the ω-plane:

$$\frac{z - z_0}{z - z_1} = \left(\frac{\xi_1 - \beta z_0}{\xi_1 - \beta z_1}\right)^{1/\beta}, \tag{1}$$

where z_1 is the position of the trailing edge point at the Z-plane and z_0 is the position of a point located half-way between the point of maximum curvature at the leading edge and its centre of curvature; β represents the parameter $\pi/(2\pi - \tau)$, in which τ is the included angle of the trailing edge.

Following the Karman–Treffez transformation, James's method[10] is used to transform the smooth quasi-circle in the ω-plane into a very accurate unit circle in the ξ-plane.

James's method makes use of a series of the form

$$\ln\left(\frac{\mathrm{d}\xi_1}{\mathrm{d}\xi}\right) = c_0 + \frac{c_1}{\xi} + \frac{c_2}{\xi^2} + \cdots, \tag{2}$$

where $c_0, c_1, c_2, \ldots$ are complex coefficients.

Truncating the series after N terms in equation (2) and applying it at equally spaced points on the circle gives

$$\ln\left(\frac{\mathrm{d}\xi_1}{\mathrm{d}\xi}\right)_j = \ln\left|\frac{\mathrm{d}\xi_1}{\mathrm{d}\xi}\right|_j + i\arg\left(\frac{\mathrm{d}\xi_1}{\mathrm{d}\xi}\right)_j = \sum_{k=0}^{N-1} c_k e^{i2\pi jk/N}, \tag{3}$$

where the subscript j identifies a discrete point on the circle, N denotes the total number of discrete points on the circle and $i = (-1)^{1/2}$.

The term on the left-hand side of equation (3) is related to the geometric variables as follows:

$$s_j = \int_0^{\omega_j} \left|\frac{\mathrm{d}\xi_1}{\mathrm{d}\xi}\right|_j \mathrm{d}\omega, \tag{4}$$

$$\arg\left(\frac{\mathrm{d}\xi_1}{\mathrm{d}\xi}\right)_j = \tau_j + \omega_j - \frac{3\pi}{2}, \tag{5}$$

where s_j is the surface arc length in the ω-plane and τ_j is the surface angle. These relationships make possible the following iteration procedure.

1. Calculate the values of τ_j and s_j at the defining points of the quasi-circle in the ξ_1-plane and determine the cubic spline coefficients of τ versus s.
2. Estimate the values of $|d\xi_1/d\xi|_j$ at equally spaced points on the circle; then perform equation (4) to obtain estimates of the values of s_j.
3. Use the cubic spline coefficients in step 1 to obtain values of τ_j corresponding to the estimated values of s_j and calculate $\arg(d\xi_1/d\xi)_j$ using equation (5).
4. Apply two successive fast Fourier transform[11] calculations, the first of which uses the estimates of $\arg(d\xi_1/d\xi)_j$ to find estimates of the coefficients in equation (3) and the second of which uses these coefficients to provide updated estimates of the values of $\ln|d\xi_1/d\xi|_j$. Then calculate the values of s_j using equation (4).
5. Repeat steps 3 and 4 until the values of $\ln|d\xi_1/d\xi|_j$ converge.

Given the coefficients of the series in equation (3), the coefficients $a_0, a_1, a_2, \ldots$ of the map function can be easily found as

$$\xi_1(\xi) = \xi + a_0 + \frac{a_1}{\xi} + \frac{a_2}{\xi^2} + \cdots. \tag{6}$$

According to equations (1) and (6), an aerofoil in the Z-plane can be conformally transformed into a unit circle in the ξ-plane.

2.2. *Conformal mapping of multi-element aerofoils*

When one aerofoil in the Z plane is transformed into a unit circle in the ξ-plane, this mapping procedure also distorts the shapes of all other nearby aerofoils. Given co-ordinates in the Z-plane, an efficient and reliable Newton–Raphson iterative method is used to solve non-linear equation (6) for co-ordinates in the ξ-plane. Then another single-element mapping procedure as described above is used to transform another aerofoil into a circle. This procedure continues until all the aerofoils in the Z-plane have been transformed into multiple circles in the ξ-plane. Because the application of the Karman–Treffez transformation makes the shapes of the multi-element aerofoils nearly circular to begin with, once a body has been transformed into a circle, subsequent mappings of other bodies have only small effects on it. The general iterative procedure for transforming multi-element aerofoils into the same number of circles has been found to converge rapidly. The procedures of mapping are shown in Figure 1.

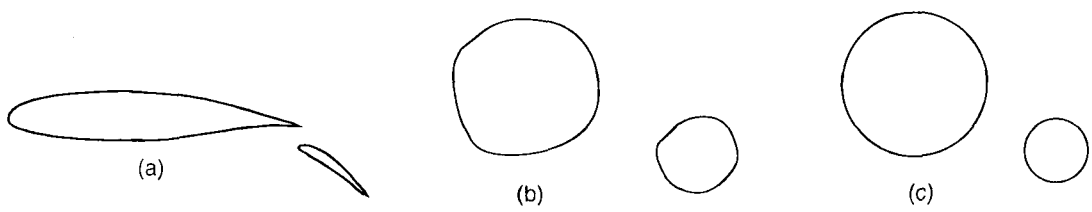

Figure 1. Transformation of a two-element aerofoil into two circles: (a) physical geometry in the Z-plane; (b) geometry in the ω-plane after Karman–Treffetz transformation; (c) two final converged circles in the ξ-plane

3. CALCULATION OF POTENTIAL FLOW IN THE ξ-PLANE

The whole transformation procedure satisfies

$$\nabla^2\phi(z) = \frac{\nabla^2\phi(\xi)}{|dz/d\xi|^2}, \tag{7}$$

$$\frac{dz}{d\xi} = \frac{dz}{d\xi_1}\frac{d\xi_1}{d\xi}, \tag{8}$$

where ϕ is the velocity potential.

The normal and tangential velocity components transform as

$$v_n(z) = \frac{v_n(\xi)}{|dz/d\xi|}, \tag{9}$$

$$v_t(z) = \frac{v_t(\xi)}{|dz/d\xi|}. \tag{10}$$

Circulation is unaffected by a conformal transformation.

If the transformation satisfies the condition

$$\lim_{|z|\to\infty}\left|\frac{dz}{d\xi}\right| = 1, \tag{11}$$

the general field equation, boundary condition and velocity condition at infinity are unchanged. The Kutta condition is also unchanged, because the present mapping derivative of the transformation is continuous across the trailing edge of each element. Thus the potential flow around the multi-element aerofoils in the Z-plane is equal to the flow around the multiple circles in the ξ-plane.

If NA is used to denote the total number of aerofoils in the Z-plane, the potential flow around the multiple circles in the ξ-plane can be decomposed into $NA + 2$ flow solutions.[12] The first two solutions have uniform flow at large distances from the circles and zero circulation at any point in the flow field. The first solution has 0° angle of attack and velocity v_x at infinity, while the second has 90° angle of attack and velocity v_y at infinity. Each of the other NA flow solutions has stagnant flow at large distances from the circles and circulation Γ_j ($j = 1, 2, \ldots, NA$) about the jth circle (zero circulation about the other circles). Reference 13 presents the analytical forms of these flow solutions for $v_x = 1$, $v_y = 1$ and $\Gamma_j = 1$ separately by using the Milne–Thomson circle theorem, which states in essence that a circle can be introduced into a flow with complex potential $\omega = f(\xi)$ by altering the complex potential to

$$\omega = f(\xi) + \bar{f}[r_0^2/(\xi - \xi_c)], \tag{12}$$

where $\bar{f}$ represents the conjugate of the function f, and r_0 and ξ_c represent the radius and centre, respectively of the circle that is introduced into the flow. By application of the Kutta condition at the points corresponding to the trailing edge points of the aerofoils in the Z-plane and application of the velocity condition at infinity, v_x, v_y and Γ_j ($j = 1, 2, \ldots, NA$) can be determined. Finally, the total potential flow around the multiple circles at a specific angle of attack can be obtained by superimposing these $NA + 2$ flow solutions.

4. CALCULATION OF BOUNDARY LAYER IN THE Z-PLANE

After the velocity distribution of potential flow in the ξ-plane has been obtained, the velocity distribution of potential flow in the Z-plane can be found from equations (9) and (10). According to this velocity distribution, the boundary layer can be calculated in the Z-plane by an integration method. For multi-element aerofoils with a large gap the effects of the confluent boundary layer are small[14] and are neglected in the present calculation. Thus the calculation of the boundary layer includes only three parts: laminar boundary layer calculation, transition calculation and turbulent boundary layer calculation. The quantities calculated are the displacement thickness δ^*, the shape factor H and the skin friction coefficient c_f. The laminar boundary layer is calculated by Cohen's method; the transition point is judged by Granvill's rule; and the turbulent boundary layer is calculated by Nash's method. Reference 15 presents these procedures in detail. In the calculation of the boundary layer here, separation is assumed to occur when the shape factor reaches $H = 2$.

5. MODEL OF SEPARATED FLOW AROUND AN AEROFOIL

For a flow with a large attack angle the separation of the boundary layer will occur somewhere on the upper surface of the aerofoil. Thus in Figure 2 separation occurs at point A on the upper surface and at the trailing edge on the lower surface of the aerofoil. Jacob's model[6] is introduced to simulate the separated region here. Along the separated surface BA, sources $q(s)$ are distributed to model the effects of separation; $q(s)$ is taken as a two-order function of s, which is the arc length from B to any point on the aerofoil surface BA. In order to make the separated stremlines AD and BD rejoin at some point D in the aft region of the aerofoil, a sink is placed at point P and the co-ordinates of P are chosen as

$$X_P = X_B + a_p, \tag{13}$$

$$Y_P = Y_M + (X_P - X_M)\tan(\beta). \tag{14}$$

Here M is the midpoint of the line AB, $a_p \approx 2l$ and $\beta = \varepsilon\alpha$, where l is the x-direction distance between the two separated points A and B and $\varepsilon \approx 0{\cdot}5$.

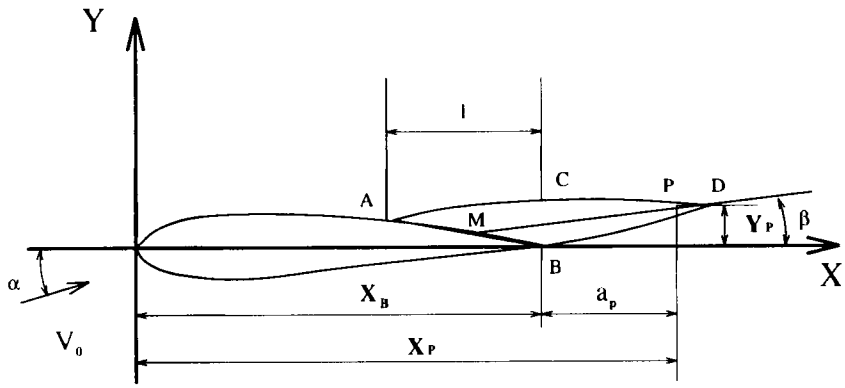

Figure 2. Jacob's model for the separated region

The strength of the sink at position P is chosen as

$$E = -\int_0^{s_A} q(s)\,\mathrm{d}s, \tag{15}$$

where s_A is the arc length of BA.

The pressure on the separated surface is determined by the semi-empirical theory that the pressure is constant in the separated region above the upper surface of the aerofoil, which can be approximately satisfied by setting

$$C_p(A) = C_p(B) = C_p(C), \tag{16}$$

where $C_p(A)$, $C_p(B)$ and $C_p(C)$ represent the pressure at points A, B and C respectively. This condition can also be used to determine the final source distribution of q.

Jacob's separated flow model which is simply described above is a semi-empirical theory mainly for engineering use. More detailed discussions about how the separated lines AD and BD, the position of sink P, the source distribution $q(s)$ and the strength of the sink at point P are chosen can be found in Reference 6.

6. ITERATIVE SOLUTION CONSIDERING THE EFFECTS OF SEPARATION

The iterative steps to find the flow solution considering the effects of separation are as follows.

1. Map the multi-element aerofoils in the Z-plane conformally on to multiple circles in the ξ-plane; then find the velocity distribution of potential flow in the ξ- and Z-planes.
2. Calculate the boundary layer of both upper and lower surfaces of the multi-element aerofoils in the Z-plane until separation occurs.
3. Distribute sources $q(s)$ on the separated surfaces of the aerofoils; simulate the displacement thickness of attached flow as an equivalent source distribution; then transform these sources on the surfaces of the aerofoils in the Z-plane into sources on the surfaces of the multiple circles in the ξ-plane. The sink at Z_P is also transformed into the sink at ξ_P.
4. Calculate the flows induced by the sources distributed on the surfaces of the circles and the sink at ξ_P; then superimpose these flows on the potential flow calculated in step 1.
5. Find the corrected v_x, v_y, source distribution $q(s)$, sink Z_P and circulation Γ_j ($j = 1, 2, \ldots, NA$) by application of equation (16), of the Kutta condition at the points corresponding to the trailing edge points of the multi-element aerofoils the Z-plane and of the velocity conditions at infinity. Then again calculate the flows induced by v_x, v_y, $q(s)$, Z_P, Γ_j ($j = 1, 2, \ldots, NA$) and superimpose these flows to obtain the total velocity distribution considering the effects of separation.
6. Repeat steps 2–5 until the stable separation points (if multiple separations occur at the surfaces of multi-element aerofoils) and pressure distribution are obtained.

In step 4 the flow induced by equivalent sources distributed on a circle is calculated as follows. When equivalent sources are determined, the boundary shape is unchanged, but the normal velocity boundary condition is changed. On the circle surface corresponding to attached flow of the aerofoil the normal velocity is given by[16]

$$v_n = \frac{\partial(v_t \delta^*)}{\partial s}, \tag{17}$$

where s is the arc co-ordinate. On the circle surface corresponding to separated flow of the aerofoil the normal velocity v_n is equal to the strength of sources distributed on that part of the surface. This induced flow also satisfies zero-flow perturbation at large distances from the circle, so the induced flow velocity can be written as

$$u - \mathrm{i}v = \frac{b_1}{\xi} + \frac{b_2}{\xi^2} + \cdots, \tag{18}$$

where $b_1, b_2, \ldots$ are complex coefficients and $\mathrm{i} = (-1)^{1/2}$.

On the surface of the circle equation (18) can also be rewritten as another formulation

$$v_n + \mathrm{i}v_t = b_1 + b_2 \mathrm{e}^{\mathrm{i}\theta} + \cdots. \tag{19}$$

Given the values of v_n at N points on the circle, it is possible in principle to determine only the first $N/2$ complex coefficients. This can be done in an efficient manner using the FFT algorithm. Given the coefficients, another FFT calculation can be used to give the v_t-values at the points on the circle. Velocity components at points off the circle are determined directly from equation (18). For the multiple circles, first the induced flow is calculated based on every single circle, then the total induced flows are obtained by superimposing them.

The flow induced by the sink at ξ_P is also calculated by using the analytical form presented in Reference 13.

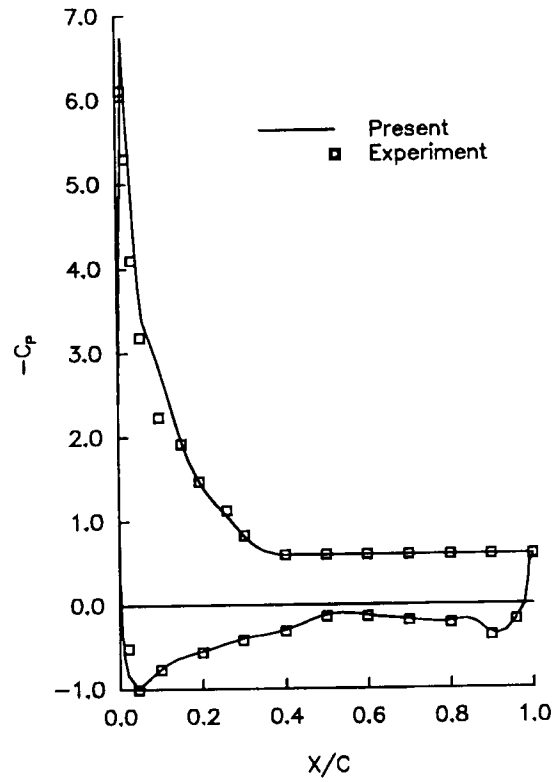

Figure 3. Comparison of pressure distributions for the GA(W)-1 single-element aerofoil ($\alpha = 18{\cdot}4°$, $Re = 2{\cdot}5 \times 10^6$)

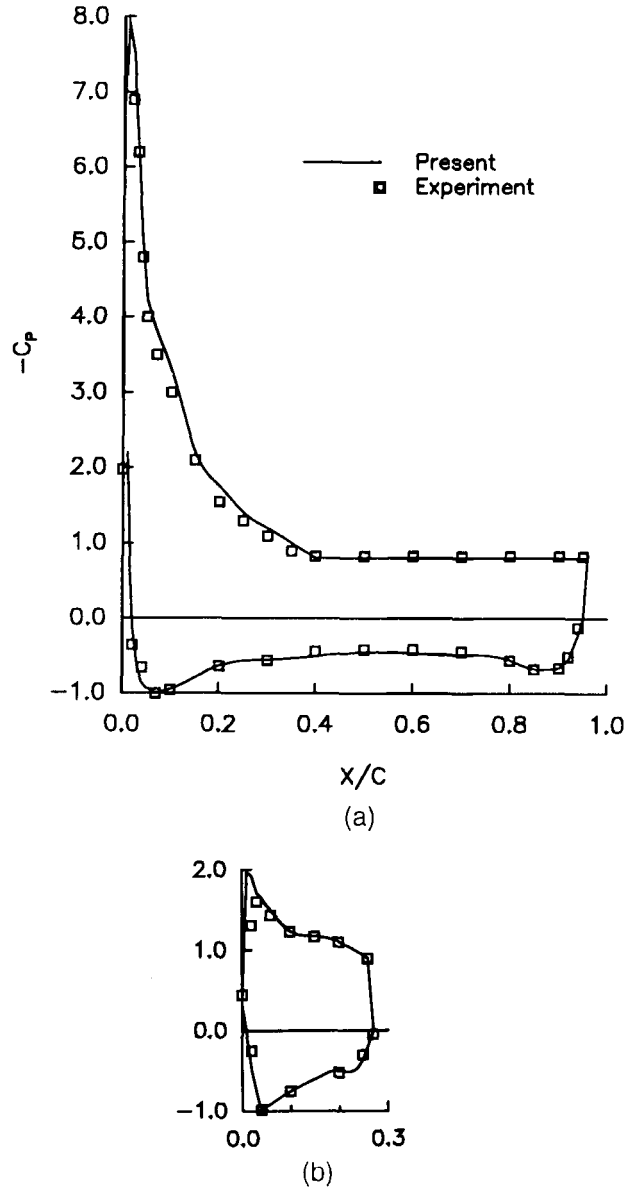

Figure 4. Comparison of pressure distributions for the GA(W)-1 two-element aerofoil (29%c model, 40° fowler flap, $\alpha = 15°$, $Re = 2{\cdot}2 \times 10^6$): (a) main aerofoil; (b) fowler flap

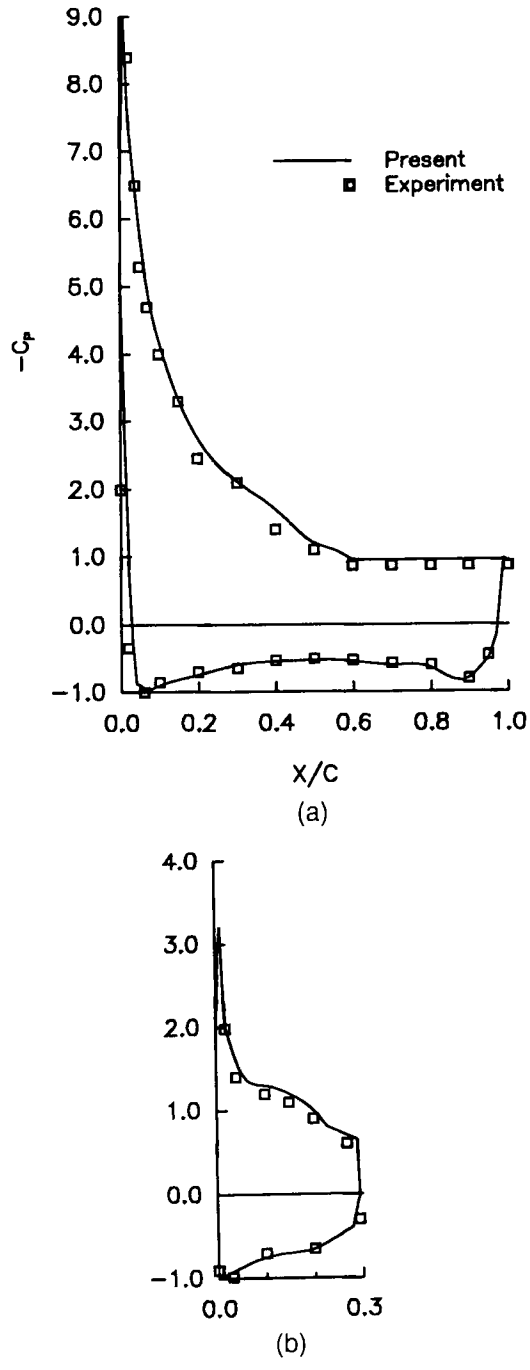

Figure 5. Comparison of pressure distributions for the GA(W)-1 two-element aerofoil (30%c model, 40° fowler flap, $\alpha = 12{\cdot}8°$, $Re = 2{\cdot}2 \times 10^6$): (a) main aerofoil; (b) fowler flap

7. RESULTS AND DISCUSSION

Using the method described above, we first study the viscous flow around the GA(W)-1 single-element aerofoil under an attack angle of 18·4°. In the numerical calculation, separation is supposed to occur at about 38%c on the upper surface of the aerofoil, while the experimental data[17] show that separation occurs at about 40%c. It is found that the variation in H from 1·8 to 2·6 has very little effect on determining the position of separation, because H increases rapidly near the separation point. Figure 3 presents the calculated pressure distribution and the experimental results on the surfaces of the GA(W)-1 aerofoil. The figure shows that the numerical results are in good agreement with the experiment results. In the iterative calculation, if N is taken as 64, it is found that about 13 iterations are needed to get a converged circle; eight iterations are needed to obtain a converged pressure distribution and a stable separation point. Because the FFT is repeatedly used in all iterative procedures, the calculation is greatly reduced.

Next, two examples of separated flow around multi-element aerofoils are studied. Figure 4 presents the comparison of calculated pressure distribution and experimental results[17] for the flow around the GA(W)-1 aerofoil with a 29%c fowler flap under an attack angle of 15°, while Figure 5 presents the comparison of calculated pressure distribution and experimental results[18] for the flow around the GA(W)-1 aerofoil with a 30%c fowler flap under an attack angle of

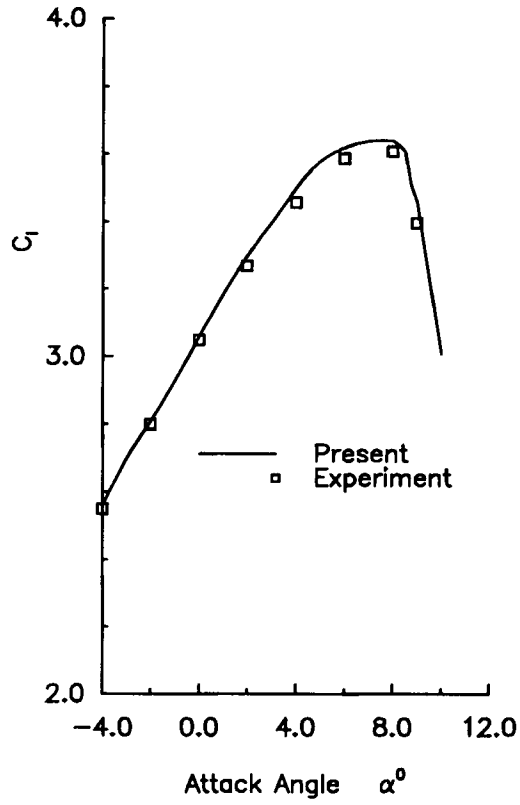

Figure 6. Comparison of lift coefficients for the GA(W)-1 two-element aerofoil (29%c model, 40° fowler flap, $Re = 2{\cdot}2 \times 10^6$)

12·8°. From these two figures it is observed that the calculated pressure distribution is generally in agreement with the experimental data, except at the leading edge of the flaps where the calculated pressure is a little higher than the experimental results. This is mainly because the effects of the confluent boundary layer are neglected in the present numerical calculation.

Finally, the lift coefficient curve for the GA(W)-1 aerofoil with a 29%c fowler flap is presented in Figure 6. The figure shows that the present numerical method can be an excellent tool for predicting the lift coefficient of multi-element aerofoils even after the occurrence of maximum lift coefficient.

8. CONCLUSIONS

A method has been presented to calculate the steady, incompressible viscous separated flow around multi-element aerofoils. On the basis of the present results, the following conclusions can be drawn.

1. Conformal mapping technique can be a very efficient tool to calculate the pressure distribution of separated flow around multi-element aerofoils.
2. This method can accurately predict the lift coefficient of multi-element aerofoils even after the occurrence of maximum lift coefficient.

REFERENCES

1. J. F. Thompson, 'Numerical solution of N–S equations for arbitrary 2-dimensional multi-element airfoils', *NASA CR 173251*, 1983.
2. M. Shigemi, 'Finite element analysis of incompressible viscous flow around single and multi-element airfoils in high Reynolds number region', *NAL TR 1010T*, National Aerospace Lab., Tokyo, 1988.
3. Z. Nemouchi, 'The computation of turbulent thin shear flows associated with flow around multi-element airfoils', *ph.D. Dissertation*, Manchester University, 1988.
4. M. Drela, 'Newton solution on coupled viscous/inviscid multi-element airfoils flows', *AIAA Paper 90-1470*, 1990.
5. D. Coiro, M. Amato and P. Mattis, 'Numerical predictions of transonic viscous flows around airfoils through an Euler/boundary layer interaction method', *Aeronaut. J.*, **96,** 157–165 (1992).
6. K. Jacob, 'Computation of separated incompressible flow around airfoil and determination of maximum lift', *AVA Rep. 67A62*, 1973.
7. G. W. Zumwalt, 'An analytical model for highly separated flow on airfoil at low speeds', *NASA CP 152702*, 1974.
8. M. L. Henderson, 'Two dimensional separated wake modeling and its use of predice maximum lift coefficient', *AIAA Paper 78-156*, 1978.
9. G. W. Zumwalt and R. Elangovan, 'Computation of low speed flow past multi-element airfoils with large flow separation', in B. Laschka and R. Staufenbiel (eds), *Proc. 13th ICAS Congr./AIAA Aircraft Systems and Technology Conf.*, Vol. 1, AIAA, New York, 1982, pp. 342–351.
10. R. M. James, 'A new look at two-dimensional incompressible airfoil theory', *Douglas Aircraft Company Rep. MD J0918/01*, 1971.
11. J. W. Cooley, 'The fast Fourier transform algorithm: programming considerations in the calculation of sine, cosine and Laplace transform', *J. Sound Vibr.*, **12,** (1970).
12. N. D. Halsey, 'Potential flow analysis of multi-element airfoils using conformal mapping', *AIAA J.*, **17,** (1979).
13. B. R. Williams, 'An exact test case for the plane potential flow about two adjacent lifting airfoils', *Aeronautical Research Council, R & M, No. 3717*, 1973.
14. W. Stevens, S. H. Goradia and J. A. Braden, 'Mathematical model for two-dimensional multi-element airfoils in viscous flow', *NASA CR 1843*, 1971.
15. G. W. Brune and D. A. Sikawi, 'Experimental investigation of the confluent boundary layer of multi-element low speed airfoils', *AIAA Paper 83-0566*, 1983.
16. N. D. Halsey, 'Conformal mapping analysis of multi-element airfoils with boundary-layer correction', *AIAA Paper 80-0069*, 1980.
17. W. H. Wentz, 'Development of a fowler flap system for a high performance General Aviation airfoil', *NASA CR-2443*, 1974.
18. H. C. Seetbaram and W. H. Wentz, 'A low speed two-dimensional study of flow separation on GA(W)-1 airfoil with 30-percent chord fowler flap' *NASA CR 2844*, 1977.